Invited Paper

Probing ultrafast electron dynamics in condensed matter with attosecond photoemission

Stefan Neppl[a], Ralph Ernstorfer[b], Adrian L. Cavalieri[c], Johannes V. Barth[d], Dietrich Menzel[d]
Ference Krausz[a], Peter Feulner[d] and Reinhard Kienberger[a]

[a]Max-Planck-Institut für Quantenoptik, 85748 Garching, Germany;
[b]Fritz-Haber-Institut der Max-Planck-Gesellschaft, 14195 Berlin, Germany;
[c]Max-Planck Research Department for Structural Dynamics, University of Hamburg, Center for Free Electron Laser Science, 22607 Hamburg, Germany;
[d]Physikdepartment E20, Technische Universität München, 85747 Garching, Germany;

ABSTRACT

We discuss experiments that address the ultrafast dynamics inherent to the photoemission process in condensed matter. In our experimental approach, an extreme ultraviolet attosecond light pulse launches photoelectron wave packets inside a solid. The subsequent emission dynamics of these photoelectrons is probed with the light field of a phase-stabilized near-infrared laser pulse. This technique is capable of resolving subtle emission delays of only a few attoseconds between electron wave packets that are released from different energy levels of the crystal. For simple metals, we show that these time shifts may be interpreted as the real-time observation of photoelectrons propagating through the crystal lattice prior to their escape into vacuum. The impact of adsorbates on the observed emission dynamics is also investigated.

Keywords: Photoemission, Surfaces, Time Delay, Ultrashort XUV Pulses, Attosecond Streaking, High-harmonic Generation

1. INTRODUCTION

The extension of established laser-based pump-probe schemes to resolve electron dynamics in the sub-fs time domain is frustrated by the natural limit for the minimum duration of a light pulse, which is set by the oscillation period of its carrier wave. This limits the duration for pulses in the near-infrared (NIR) and ultraviolet spectral range to a few femtoseconds, and restricts the prospects of breaking the femtosecond barrier for the pulse duration to the shorter wavelength part of the electromagnetic spectrum. Over the last decade, tremendous progress in laser technology made it possible to produce highly intense laser pulses in the NIR spectral region with durations approaching this single-cycle limit, and even enabled control of the electric field within the pulse envelope.[1,2] When atoms are exposed to such intense light fields, they can be forced to emit high harmonics of the fundamental laser frequency in form of isolated bursts of extreme-ultraviolet (XUV) radiation, with durations significantly shorter than the period of the NIR driver pulses.[3,4] Further improvements and developments resulted in the generation of XUV pulses with durations of only 80 as (1 as = 10^{-18} s), which opened the door for time-resolved spectroscopy with unprecedented temporal resolution.[5] Applied to simple atomic systems in the gas-phase, the combination of attosecond XUV pulses with inherently synchronized NIR laser pulses has enabled the real-time observation of field-induced electron tunneling,[6] the study of valence electron wave packet motion,[7] and the discovery of subtle time delays in the photoemission from different atomic orbitals.[8]

However, many fundamental and technologically relevant sub-fs phenomena, like interfacial charge transfer,[9] electronic screening[10] and atomic-scale electron transport take place in the solid-state. Despite these promising prospects, time-domain attosecond spectroscopy of condensed matter was only recently demonstrated by extending the attosecond streaking methodology to solid surfaces. In attosecond streaking, one-photon photoemission

Correspondence should be addressed to S.Neppl (stefan.neppl@mpq.mpg.de)

Ultrafast Phenomena and Nanophotonics XVII, edited by Markus Betz, Abdulhakem Y. Elezzabi, Jin-Joo Song, Kong-Thon Tsen, Proc. of SPIE Vol. 8623, 862312 · © 2013 SPIE · CCC code: 0277-786X/13/$18
doi: 10.1117/12.2003050

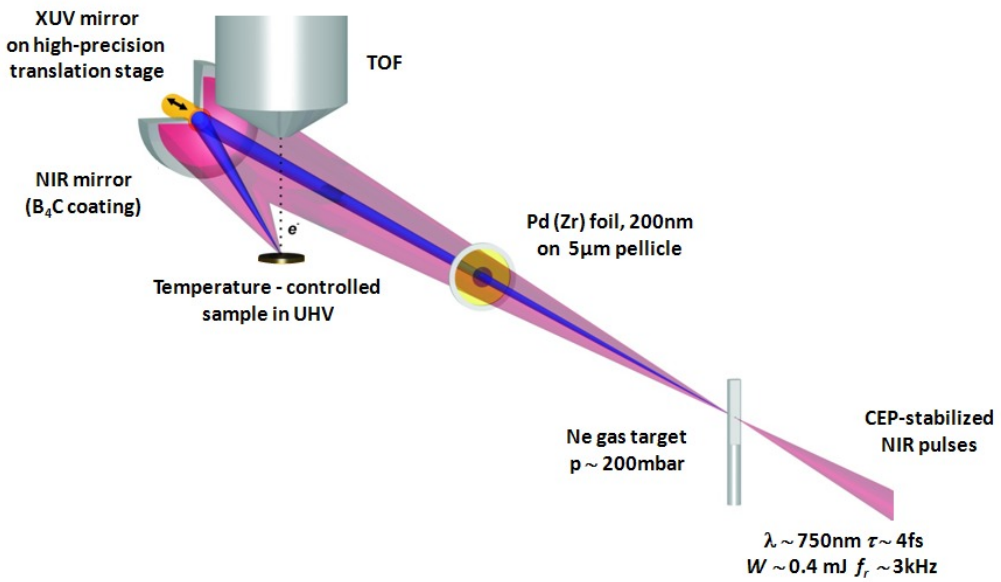

Figure 1. Schematic depiction of the setup allowing attosecond streaking experiments on surfaces. See text for details.

is initiated by an isolated attosecond XUV pulse, and the outgoing photoelectron wave packets are streaked by a waveform-controlled NIR laser field as the relative delay between both light fields is varied.[11,12] The resulting spectrograms provide access to both the temporal structure and relative time delays in the release of these electrons, which are mapped onto corresponding relative shifts between their NIR-modulated energy spectra.[8,13] A first proof-of-principle experiment revealed that the XUV-induced photoemission from a tungsten (110) surface features an intriguing temporal structure which is determined by the motion and interaction of the photo-excited electrons prior to their escape from the solid. Using the electric field of an NIR pulse as a probe, Cavalieri *et al.* measured a relative time delay of 110 ± 70 as between the ejection of photoelectrons from the valence band and the $4f$ core levels of the crystal.[13] Unfortunately, the complexity of both the employed spectroscopic technique and the many-body interactions inherent to photo-excitation and electron propagation in condensed matter complicate a conclusive explanation of these time shifts so far.[14–18]

In order to shed light on the mechanisms underlying this phenomenon in condensed matter, we performed similar experiments on different single crystals and well-defined metal-adsorbate interfaces. We demonstrate the capability of the attosecond streaking method for clocking electron emission from solids with a precision of only a few attoseconds. Our results further indicate that, for metals exhibiting a nearly free-electron-like electronic band structure, the measured time delays can be intuitively related to the propagation of the photoelectrons inside the solid prior to their escape through the surface. This holds true irrespective of the spatial localization of their initial electronic wave function - in strong disagreement with predictions from full quantum mechanical calculations.[14,16,18,19] In the following section, we briefly introduce some experimental concepts and the infrastructure necessary for attosecond streaking experiments. Recent results obtained with this method from clean and adsorbate-covered surfaces are discussed in Section 3. A short summary will be given in Section 4.

2. EXPERIMENT

Time-resolved experiments of solid surfaces based on the attosecond streaking principle require a sophisticated infrastructure starting with a laser system delivering ultrashort, intense, waveform-controlled laser pulses, a setup for high-harmonic up-conversion of these optical pulses into the XUV spectral range, suitable filtering of this radiation to isolate single sub-fs XUV pulses, and finally an experimental station allowing the preparation and

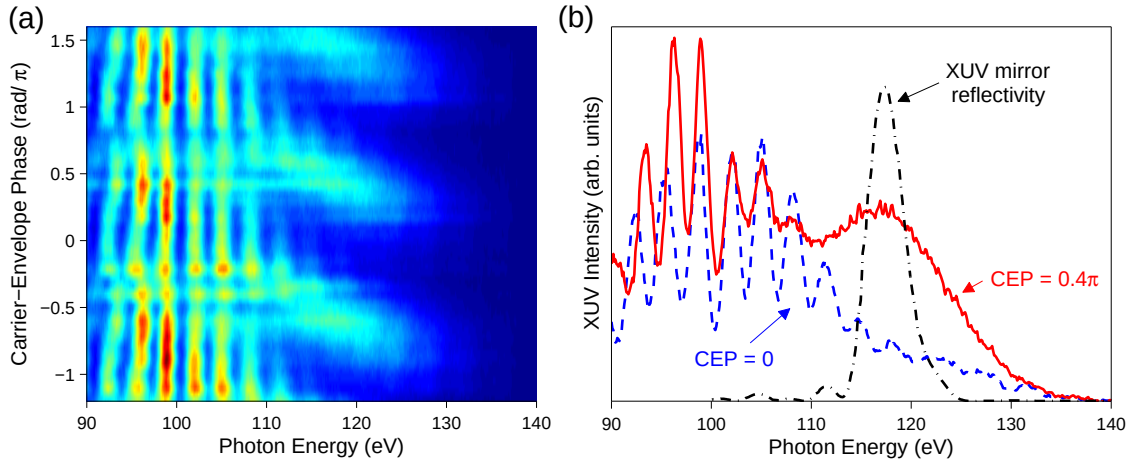

Figure 2. High-harmonic generation in neon by sub-5 fs NIR laser pulses. (a) High-harmonic spectra as a function of the carrier-envelope-phase (CEP) of the driving laser pulse. (b) Comparison of high-harmonic spectra for CEP=0 (blue dashed line) and CEP= 0.4π (red solid line). The latter waveform produces the most intense continuum of XUV radiation. In this case, the generated continuum ranges from ∼110 eV to ∼130 eV, which supports isolated attosecond pulses with Fourier-limited pulse durations down to 100 as. A typical reflectivity curve of a multilayer mirror used in our streaking experiments to filter sub-fs XUV pulses is also indicated (black dashed-dotted line).

spectroscopic investigation of well-defined, atomically clean solid-state samples under ultra-high vacuum (UHV) conditions. The latter is mandatory considering the high surface sensitivity of photoemission in the XUV range, which has higher requirements on vacuum conditions than implemented in previous state-of-the-art attosecond pump-probe setups, which have primarily been developed for experiments in the gas phase.

A schematic overview of our apparatus is presented in Fig 1. Few-cycle, ∼0.4 mJ NIR laser pulses (violet beam) with a carrier wavelength of ∼750 nm are produced by an amplified 3 kHz Ti:sapphire laser system and focused into a neon-filled gas target to generate a collinear beam of coherent XUV radiation (blue beam) via high harmonic generation (HHG).[2,20] This broadband and low-divergent XUV radiation is spatially separated from the fundamental NIR light by a thin metal filter in the center of the beam path. After their spatial separation, the annular NIR beam and the central XUV beam enter an experimental chamber maintained at a base pressure below $5 \cdot 10^{-11}$ mbar. In this chamber, both beams are reflected by a coaxial assembly of two spherical mirrors ($f = 12.5$ cm) and focused onto the surface of a temperature-controlled solid-state sample. The inner mirror is coated with a dedicated multilayer structure acting as a bandpass filter for the incident XUV radiation. It is further attached to a piezo-electric translation stage that allows to introduce a delay between the XUV and the NIR pulses, which are reflected by the fixed outer mirror (coated with boron carbide). The UHV chamber accommodates additional equipment for *in vacuo* crystal cleaning and controlled layer growth: an ion sputter gun, a four-grid back-view LEED (low-energy electron diffraction) system, a Knudsen-type effusion cell, a quadrupole mass analyzer for thermal desorption studies, and a gas dosing system. A more detailed description of the experimental setup has been presented elsewhere.[21] In the actual streaking measurement, the kinetic energies of the XUV-induced photoelectrons, which are emitted from the crystal surface along the NIR laser polarization, are analyzed by a time-of-flight spectrometer (TOF) as a function of the relative delay between the NIR and XUV pulses.

The most essential part in producing attosecond light pulses is the process of HHG. It involves ionization and recombination dynamics of valence electrons detached from the neon atoms in the gas target, which are driven by the high electric field-strength of the fundamental NIR pulses. The basic mechanism can be understood within a semi-classical model, where the process is divided into three sequential steps.[22] In the first step, a weakly bound valence electron is detached from the atom by tunnel ionization. This happens most efficiently around the

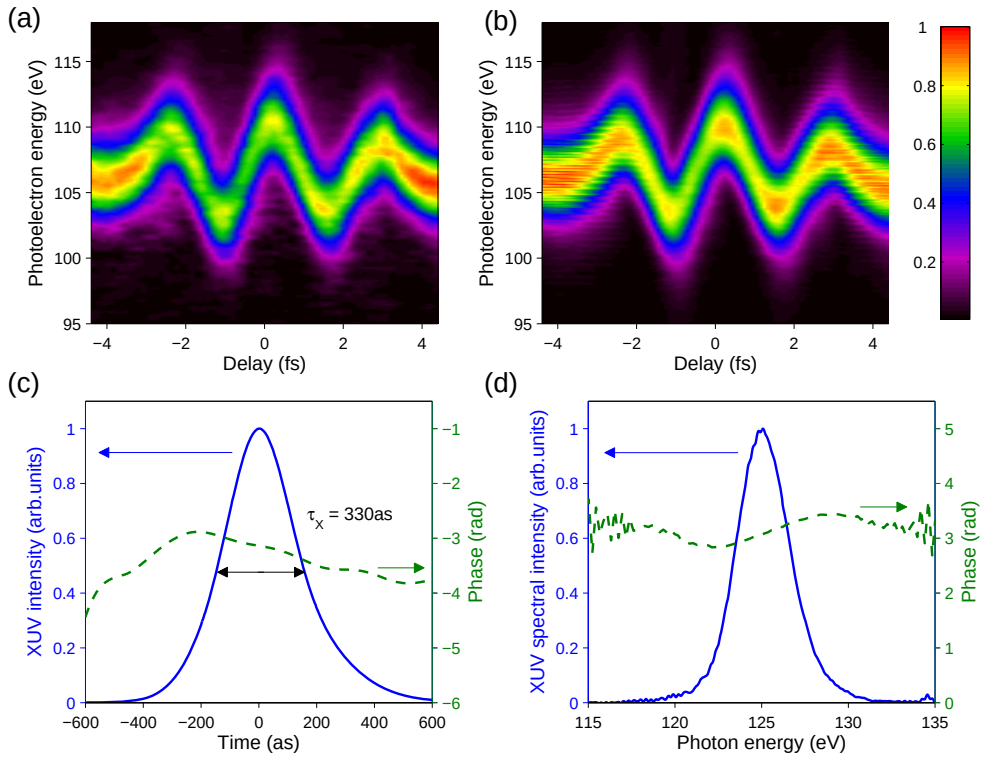

Figure 3. Characterization of a sub-400 as XUV pulse by streaking Ga3*d* photoelectrons emitted from a sputter-cleaned GaAs(100) surface. (a) Measured streaking spectrogram. The XUV pulses were filtered from the high-harmonic cut-off continuum with a multilayer mirror reflecting incident radiation at 125 eV over a bandwidth of ∼6 eV. The delay between the generated XUV pulse and the NIR laser field was varied in steps of 100 as. The corresponding spectrogram reconstructed after 5×10^3 iteration by a FROG algorithm, specially tailored for attosecond streaking experiments,[23] is shown in (b). Panels (c) and (d) show the retrieved attosecond XUV pulse (blue solid line) and the retrieved phase (green dashed line) in the temporal and spectral domain, respectively.

crests of the NIR field oscillations, where the instantaneous electric field is strong enough to substantially deform the atomic Coulomb potential. Once freed from the atomic potential, the electron is accelerated away from the nucleus like a classical particle in the laser field. A quarter of an optical cycle after ionization, the electric field reverses its direction and the electron is driven back to its parent ion with a small probability to recombine. The energy gained by the electron during its excursion in the laser field (plus the ionization potential of the atom) are then released in the form of a short burst of high energy photons as the atom relaxes to its ground state. Since both the ionization and recombination of the electrons happens within a fraction of a half-cycle of the NIR driving field, the emitted radiation will have a sub-fs temporal structure. Generally, when many-cycle NIR driving pulses that feature several field maxima of comparable strength are used for HHG, a train of sub-fs XUV pulses will result. However, for attosecond streaking spectroscopy, isolated sub-fs XUV pulses are needed. This can be achieved by using sub-2-cycle NIR pulses that exhibit only one dominant maximum of the electric field. In this way, the generation of the highest photon energies is restricted to a single electron re-collision event. In the frequency domain, this corresponds to a disappearance of the discrete harmonic structure for the highest orders (the so-called cut-off region), and the formation of a smooth spectral continuum.[2] An isolated attosecond pulse can then be obtained by spectral filtering this cut-off continuum by suitable multilayer mirrors.[5]

Since the temporal evolution of the electric field within a short laser pulses changes dramatically with the

phase between the carrier wave and its intensity envelope (the so-called carrier-envelope phase (CEP)), it will strongly influence the efficiency of the HHG process and the production of attosecond XUV pulses. This effect is illustrated in Fig. 2, which shows high-harmonic spectra generated with our apparatus for different settings of the CEP of the sub-5 fs NIR driver pulses. In accordance with previous observations,[5,20] the XUV continuum is maintained for almost all CEP settings. Moreover, for CEPs close to 0.4π, the intensity of the cut-off continuum is significantly enhanced, and extends over an energy range of more than 20 eV. If this part of the XUV spectrum is properly filtered, isolated attosecond pulses with a Fourier-limited pulse duration of 100 as can be generated. This is in contrast to HHG driven by NIR pulses with durations of ∼6-20 fs, where the generation of isolated attosecond pulses strictly requires a cosine waveform (i.e. CEP = 0).

In our attosecond photoemission experiments, we employ mulilayer mirrors with reflectivity bandwidths in the range of 4-6 eV, which translates into XUV pulse durations of 450-300 as. With these parameters, we can make full use of the high temporal resolution provided by the attosecond streaking method while, at the same time, retaining the necessary spectral resolution to discriminate between photoemission from different energy levels of the solid. An exemplary characterization of a 330 as XUV pulse with a central energy of ∼125 eV is summarized in Fig. 3. In this streaking measurement, Ga3*d* electrons emitted by the XUV pulse from the surface of a sputter-cleaned GaAs(100) wafer were streaked by the electric filed of the sub-5 fs fundamental NIR pulse. Since a streaking experiment can be interpreted as a cross-correlation between the XUV-induced photoelectron wave packet and the vector potential of the NIR streaking field, a FROG-type fit algorithm can be used retrieve the XUV pulse properties. This analysis reveals the successful generation of nearly bandwidth-limited XUV pulses with a negligible group-delay-dispersion of less than 1000 as^2.

3. RESULTS AND DISCUSSION

3.1 Attosecond photoemission from a clean metal surface

The proof-of-principle experiment on tungsten[13] motivated several theoretical studies[14–18,24,25] with the goal to identify the origin of the observed time delay $\Delta\tau$. However, a first-principles description of the process is challenging, as it requires the calculation of the electronic and optical many-body response of an extended system to two spectrally separated light pulses on the attosecond timescale. The inevitable simplification of the problem currently allows for various theoretical approaches which result in different, partly contradictory explanations of the observed time shift. When prompt screening of the NIR field at the solid-vacuum interface is assumed, $\Delta\tau$ may be interpreted in a simple semi-classical picture as the difference between the average travel times $\tau_{t,i} = \lambda_i/v_i$ needed by photoelectrons emitted from distinct energy levels i to reach the surface of the crystal, where they are exposed to the streaking field.[13,15] Here, λ_i denotes the mean electron escape depth and v_i is the group velocity of the photoelectrons inside the solid. Originally, a strong deviation of v_i from free-electron-like final-state dispersion was proposed to cause the main contribution to $\Delta\tau$.[13]

A conceptually rather different explanation was derived from a full quantum-mechanical treatment of the problem. In these models, $\Delta\tau$ arises from the different spatial localization of core and valence initial states independent of any final-state effects.[14,16,24] In a very recent description of the phenomenon, sizable time delays in photoemission are predicted to occur near final-state band gaps − even for situations where the NIR penetration depth exceeds the escape depth of the emitted electrons.[17] Despite the use of significantly different approximations, all theoretical approaches currently reproduce the measured time delay for W(110) within the experimental error, which calls for additional measurements on theoretically more accessible systems. We therefore performed attosecond streaking experiments on the (0001) surface of magnesium, which exhibits a much simpler electronic band structure than tungsten. Due to its nearly free-electron-like initial- and final-state dispersion,[26,27] uncertainties in assigning group-velocities to the propagating electrons are minimized. Furthermore, the dielectric response of this free-electron metal can be assumed to result in an efficient screening of the NIR streaking field at the first atomic layer.[28]

From the experimental point of view, however, streaking experiments on magnesium are more challenging than on tungsten. This is partly due to the much higher reactivity of magnesium (Mg), which limits the data

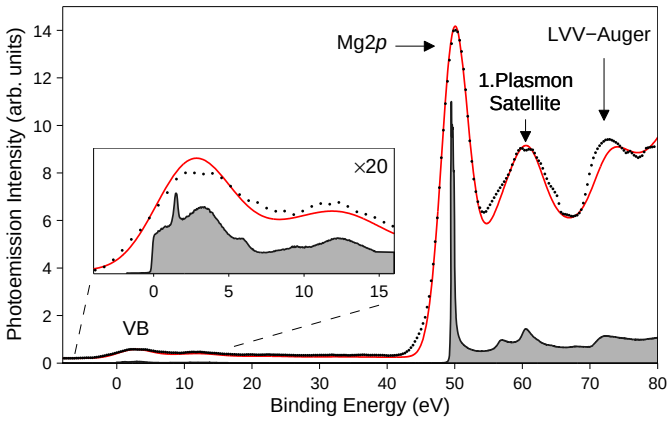

Figure 4. Stationary photoemission from Mg(0001). A synchrotron photoemission spectrum at $\hbar\omega = 120$ eV (gray shaded area) is compared to spectrum obtained with ∼400 as XUV pulses centered at ∼120 eV (black dotted line). The inset provides an enlarged view of the valence band (VB) emission. A convolution of the synchrotron spectrum with the reflectivity response of the XUV mirror employed in the attosecond experiment is shown as red solid line.

acquisition times. Furthermore, the cleaning procedures necessary to prepare well-ordered and atomically clean surfaces from this material are rather time consuming, which complicates the handling of Mg single crystals in streaking experiments. We therefore persued a different approach based on *in situ* deposition of Mg atoms. Mg was sublimated at a rate of 10 ML/min from a Knudsen-cell evaporator onto a freshly cleaned W(110) surface. It is well known that these eptiaxial Mg films exhibit geometric and electronic properties indistinguishable from Mg(0001) single crystals for layer thicknesses exceeding 20 ML.[27] Figure 4 compares the photoemission from a 30 ML magnesium sample excited with $\hbar\omega = 120$ eV synchrotron radiation (gray shaded area) to a corresponding spectrum recorded with 400 as, 120 eV attosecond pulses (black dotted line). The latter is in good agreement with a convolution (red line) of the synchrotron data and the reflectivity bandwidth of the employed multilayer mirror.

For an excitation energy of ∼120 eV, the photoemission from Mg(0001) is dominated by the $2p$ core states at a binding energy of ∼49.5 eV. As expected from the small atomic photo-ionization cross-section of the Mg$3s$ levels and the low density of states near the Fermi level for *sp*-metals, the intensity of the valence band (VB) photoemission is rather small which presents a further challenge for streaking experiments on this system. The VB comprises mainly bulk transitions for binding energies < 6 eV.[26,29] The weaker features in the binding energy range of $7-15$ eV can be ascribed to satellites produced by surface- and bulk-plasmon excitations accompanying the main transitions.[30] The sharp emission line at 1.6 eV binding energy stems from the localized Γ-surface-state, whose contribution to the total VB emission is negligible at this photon energy,[26,27] which further simplifies the interpretation of the VB photoelectron wave packets launched from this system in a streaking experiment. The plasmon loss lines are even more pronounced for the $2p$ emission, which explains the broad peak at ∼60 eV binding energy. Most importantly, the Auger electrons resulting from the decay of the $2p$ core holes appear in a binding energy range > 70 eV, and do therefore not obscure the primary $2p$ and VB emission.

For the attosecond streaking measurements, the XUV-induced photoemission is simultaneously dressed by a 10^{11} W/cm^2 strong NIR field. At this excitation level, above-threshold electrons originating from multi-photon absorption from the NIR pulse are effectively confined to kinetic energies < 40 eV. The background of inelastically scattered electrons in the spectral region of interest could therefore be removed based on the Shirley method.[31] The final background-corrected streaking spectrogram, shown in Fig. 5(a), is compiled from 40 individual photoemission spectra with the relative delay τ between the NIR and XUV pulses varied in

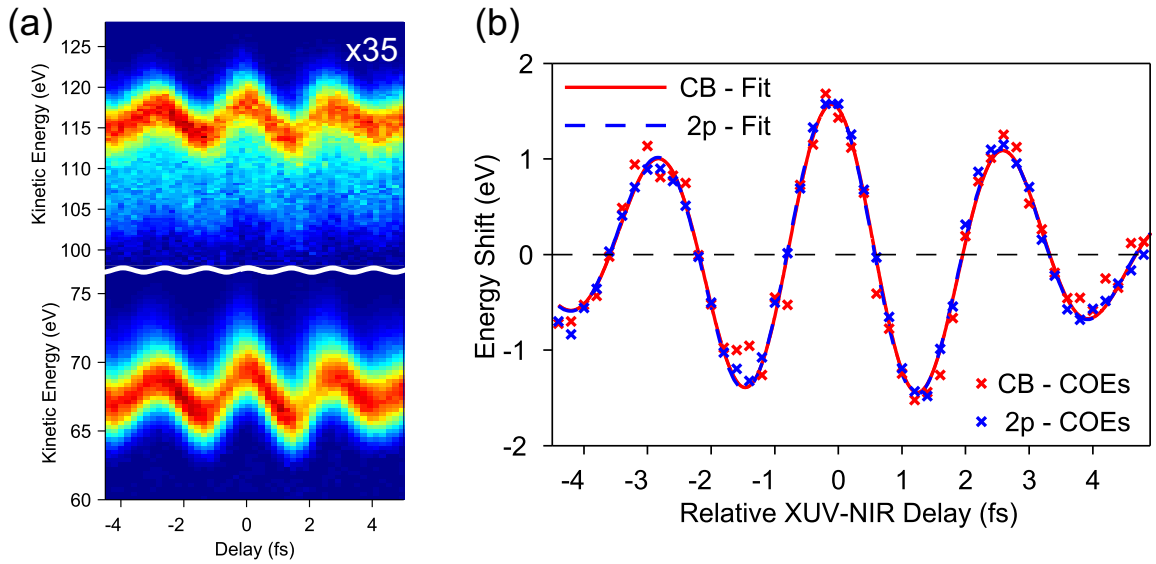

Figure 5. Attosecond time-resolved photoemission from the clean Mg(0001) surface. Isolated sub-fs XUV pulses centered at ∼120 eV are filtered with a 4.5 eV broad multilayer bandpass from the cut-off continuum and excite electrons from the Mg2p and the VB states in the presence of a 10^{11} W/cm^2 strong NIR streaking field. (a) Measured streaking spectrogram compiled from 40 individual spectra, each integrated over $\sim 1.4 \cdot 10^5$ laser shots. The VB region is scaled by $\times 35$ to visualize the good signal-to-noise ratio. (b) Timing analysis of the photoemission. Calculated center-of-energies (COEs) for the VB and 2p region (depicted as crosses) are fitted to a pair of parametrized analytic function describing the vector potential of the NIR streaking pulse. The absence of a relative shift between the fitted functions, shown as red solid line for the VB and blue dotted line for the 2p emission, provides evidence for a synchronous release of these electrons from the metal surface.[19]

increments of 150 as. Clearly, both the VB and 2p electron distributions exhibit the characteristic oscillations following the time evolution of the NIR vector potential $A_L(t)$.

As mentioned in Section 1, any time delay between the release of photoelectron wave packets from the surface should manifest itself in a relative shift between the respective parts in the spectrogram.[8,13] Obviously, such an offset cannot be inferred from simple inspection of the raw data, even when the two spectral regions are normalized to the same intensity as in Fig. 5(a). A quantitative analysis can be based on comparing the first moments $E_{COE}(\tau)$ (also called center-of-energies (COE)) calculated for the corresponding regions of the spectrogram $P(E,\tau)$ as a function of τ according to:

$$E_{COE}(\tau) = \frac{\int_{E_{min}}^{E_{max}} P(E,\tau) E \, dE}{\int_{E_{min}}^{E_{max}} P(E,\tau) dE} - E_0, \tag{1}$$

where E_{min} =100(60) eV and E_{max} =125(75) eV for the VB(2p) electrons. E_0 denotes the corresponding COE for a spectrum recorded far from temporal NIR-XUV overlap. Analyzing streaking spectrograms with this COE method has the advantage that no peak shape for the photoemission lines has to be specified. The results are shown as crosses in Fig.5(b). Apparently, both $E_{COE}(\tau)$-traces oscillate perfectly in phase without any discernible relative offset $\Delta\tau$ along the NIR-XUV delay axis. We further verify the absence of a time delay between the emission of VB and the 2p by simultaneously fitting their streaking traces to the same parametrized waveform:

$$A_L(\tau) = A_0 \, e^{-2\ln 2(\tau/\tau_L)^2} \sin(\omega_L \tau + \varphi_0) \tag{2}$$

that describes the NIR vector potential (solid lines in Fig.5(b)).

We begin our discussion of this simultaneous release of the VB and $2p$ electrons from Mg(0001) by noting that the refractive index of this material is smaller than unity over the entire spectral bandwidth covered by the NIR pulses.[32] This implies their total reflection at the metal surface for the grazing incidence condition in our experiment. Thanks to the strongly damped evanescent wave within the bulk, the assumption that the streaking field disappears inside the metal seems therefore to be even better justified than in the case of W(110).[28] Moreover, the band structure of Mg for final-state energies above 30 eV is well described by a free-electron parabola.[26] It is therefore appropriate to estimate the average travel times τ_t of the VB and $2p$ electrons towards the surface using their free-particle velocities $v_i = \sqrt{2E_i/m_e}$ and the free electron mass m_e. Taking the escape depths for ∼115 eV ($\lambda_{VB} = 5.9$ Å) and ∼68 eV electrons ($\lambda_{2p} = 4.8$ Å) in Mg,[33] we find identical propagation times $\tau_t = 92$ as for *both* types of electrons.

This effect of cancellation between the electron's velocities and escape depths λ, which results in a vanishing relative time delay in their release, is a general consequence of the monotonic increase of λ in the energy interval of $60 - 120$ eV. Although our experimental finding can be explained within a very simple heuristic model for electron propagation, it is *at variance* with recent quantum-mechanical calculations that predict pronounced time shifts of ∼100 as solely arising from a large difference in the initial-state localization of the probed electronic levels.[14,16,24] Compared to the previously studied W(110) system, where the narrow $5d$-derived bands imply an at least partly localized character of the VB states, Mg(0001) with its completely delocalized and free-electron-like dispersing VB electrons[26,27] has to be considered as an even better benchmark for testing these models. The disagreement between theory and experiment in the case of Mg points therefore to a deficiency in the current quantum mechanical description of the attosecond dynamics accompanying the photoemission in solids.

3.2 Adsorbate effect in attosecond photoemission from solids

The adsorption of atoms on a surface can lead to changes in the electronic structure in the surface-near region, and is often accompanied by a rearrangement of the valence charge density within the topmost layers of a solid. Depending on the strength of interaction, the adsorbate valence levels will either remain localized and almost unperturbed, or they may hybridize with band states of the substrate leading to the formation of new electronic states which can be significantly delocalized across the interface region. The presence of a chemically different species on a metal surface can therefore influence the initial-state character of the conduction band electrons which contribute to the measured photoemission current. On the other hand, the wave functions of the stronger bound core electrons in the substrate will remain unaffected by the adsorption process (besides a small shift of the core-level energies at the very surface). In particular, the spatial extent of their wave functions will hardly be perturbed. This fundamentally different behavior upon adsorption should be reflected in the time structure of electrons released from these two types of electronic states. In the following, we search for such an adsorbate-induced effect in a highly-ordered monolayer of oxygen atoms adsorbed on the (110) surface of tungsten.

The oxygen monolayer was prepared by exposing the freshly cleaned W(110) surface to ∼1000 L O_2 with the sample temperature raised to ∼1000 K. Under this conditions, oxygen is known to chemisorb atomically in the three-fold hollow sites of the W(110) plane forming a densely-packed layer with (1×1) symmetry.[34–37] Further, no bulk oxidation or adsorbate-induced reconstruction of the W(110) surface occurs during this surface reaction. The (110) surface of a bcc crystal offers two possible triply-coordinated adsorption sites per surface unit cell which cannot be occupied by the oxygen atoms simultaneously, therefore giving rise to the formation of two different types of domains. For high-temperature adsorption, an additional ordering of the oxygen layer can be observed which is characterized by a regular spacing of the $[\bar{1}\,1\,2]$ and $[1\,\bar{1}\,2]$ domain walls in the $[1\,\bar{1}\,1]$ and $[1\,\bar{1}\,\bar{1}]$ direction [35–37]. This additional periodicity manifests itself in the corresponding LEED pattern (see Fig.6(c)) as a set of superstructure spots superimposed on the (1×1) pattern and trailing off in the $[1\,\bar{1}\,1]$ and $[1\,\bar{1}\,\bar{1}]$ direction. The chemisorption of oxygen also induces pronounced changes in the electronic structure of W(110). This can be resolved even with our broadband attosecond XUV pulses, as demonstrated in Fig.6(a). For the clean tungsten surface, the spectrum is characterized by the $4f$ core-level emission at kinetic energies around ∼85 eV, and the weaker emission from the $5d$-dominated valence band. Upon oxygen adsorption, the $4f$ emission

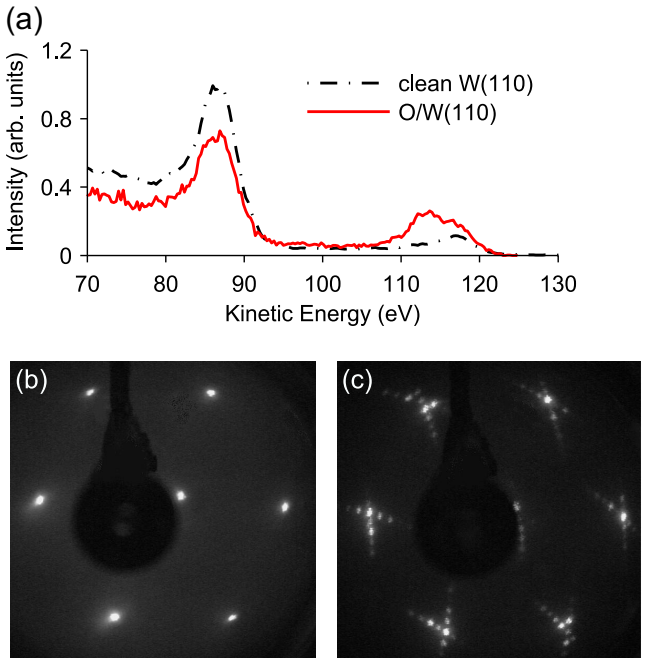

Figure 6. Effects of oxygen adsorption on the W(110) surface. (a) Stationary photoemission obtained with ∼400 as XUV pulses (120 eV central energy) from W(110) before (black dashed-dotted line) and after adsorption of 1ML oxygen (red solid line). Representative LEED patterns obtained from the clean and oxygen-covered W(110) surface are shown in (b) and (c), respectively.

is slightly attenuated while the signal from the valence band is enhanced and broadened towards lower kinetic energies. This is due to the presence of O2p-derived electronic states which have a binding energy of ∼6 eV. In order to investigate the impact of oxygen-adsorption on the emission dynamics of the excited electrons, we compared streaking measurements conducted on the clean and oxygen-covered surface. Representative streaking spectrograms are shown in Fig.7(a) and (c), respectively. The corresponding COE analysis of the emission lines are presented in panel (b) and (d). Obviously, the time shift between the VB and $4f$ photoemission increases from $\Delta\tau$ ∼30 as to $\Delta\tau$ ∼90 as in the presence of the adsorbate layer.

The interpretation of this adsorbate-induced effect touches upon several fundamental issues. In general, changes in the electronic structure of a solid are inextricably linked to a corresponding change of its optical properties via the dielectric function. This has two main implications for the interpretation of attosecond streaking experiments on adsorbate-covered surfaces. Firstly, the initial as well as the final states defining the properties of the released electron wave packets can differ from the pristine case. Secondly, modifications of the NIR streaking field at the newly formed interface due to changes in refraction and screening have to be taken into account. Although the notion of screening and refraction is debatable when applied on atomic length scales, two scenarios might nevertheless be distinguished:

1. if the NIR screening efficiency of the adsorbate layer is much weaker than for the substrate, the photoelectrons excited inside the adsorbate can be considered to experience instantaneously the full strength of streaking field, i.e. similar to the situation in gas-phase experiments. Measuring the streaking time delay between these photoelectrons and those originating from the underlying substrate would then reveal the average travel time τ_t of the substrate electrons to the substrate-adsorbate interface, which in our case corresponds to ca. 80 as for the $4f$ electrons. Strictly speaking, this is only correct when the VB emission is completely dominated by the O2p levels.

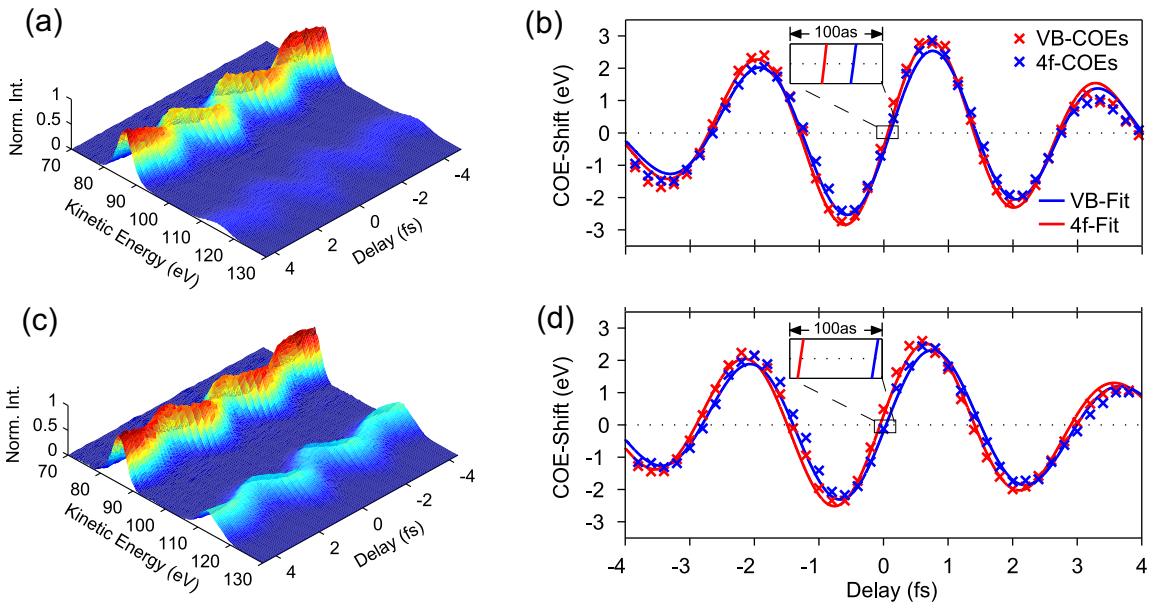

Figure 7. Influence of adsorbates on the attosecond dynamics of photoemission from W(110). Representative streaking spectrograms obtained from W(110) before and after saturation of the surface with one monolayer of atomic oxygen are depicted in (a) and (c), respectively. The relative delay between the IR and XUV light pulses is varied in steps of 200 as. For each delay step, a Shirley-type background was iteratively calculated and subtracted from the raw photoelectron spectrum. The corresponding time-domain analysis of the streaked VB and W4f photoemission via the COE method is summarized in panel (b) for the clean surface and in (d) for the oxygen-covered surface, respectively. Insets span a total IR-XUV delay range of 100 as and highlight the enhanced photoemission time shift upon oxygen adsorption.[38]

2. if on the other hand the screening efficiency of the overlayer is similar to the substrate material, the apparent travel time of the substrate electrons will be increased at least by the time required to traverse the 0.1 nm thick oxygen layer, which amounts to only ∼20 as in the case of the 4f electrons. However, the relative emission delay between the 4f core-level and the hybrid O2p-W5d VB will be further increased, since the O2p initial-states are located closer to the vacuum than 5d states and make the dominant contribution to the VB emission (see Fig.6(a)).

Apparently, the oxygen-enhanced time delay can be explained within both scenarios. However, the second scenario might be more realistic, since the the high electronegativity of oxygen provokes a partial charge transfer from the topmost layers of W(110) towards the adsorbate, which will tend to screen the NIR streaking field inside the oxygen layer.

4. SUMMARY

In conclusion, we applied attosecond time-resolved photoemission spectroscopy to the simple, free-electron metal magnesium, which should be more amenable to theoretical investigations compared to the previously investigated transition metal tungsten. In this system, valence-band and core-level photoelectrons are found to be emitted essentially simultaneously from the crystal surface. Our result indicates that transport-related contributions to attosecond time delays in solid-state photoemission may be satisfactorily explained by the knowledge of the electron wave packet's group velocities and their mean free path in the material – irrespective of the spatial localization of the initial states. This will facilitate the interpretation of time-resolved experiments on more complex phenomena like charge transfer or screening, where electron correlation is expected to further influence

the release dynamics of the excited electrons on an attosecond time scale. We have also demonstrated that the emission dynamics of the photoelectrons can be significantly affected by adsorbates on the crystal surface. This strong adsorbate effect has important implications for future attosecond photoemission experiments on clean metal surfaces, since even traces of impurity atoms in the surface-near region might be sufficient to alter the measured time delays.

ACKNOWLEDGMENTS

We thank E. Magerl, M. Stanislawski, M. Hofstetter, A. Guggenmos and N. Karpowicz for earlier contributions to the experimental setup and the data analysis. S.N. and P.F. acknowledge financial support by the Munich Center of Advanced Photonics (Project B.1.4) and thank the staff of BESSY-II for technical assistance during the synchrotron photoemission experiments. R.K. acknowledges funding from an ERC Starting Grant.

REFERENCES

[1] Brabec, T. and Krausz, F., "Intense few-cycle laser fields: Frontiers of nonlinear optics," *Rev. Mod. Phys.* **72**, 545 (Apr. 2000).

[2] Baltuška, A., Udem, T., Uiberacker, M., Hentschel, M., Goulielmakis, E., Gohle, C., Holzwarth, R., Yakovlev, V. S., Scrinzi, A., Hänsch, T. W., and Krausz, F., "Attosecond control of electronic processes by intense light fields," *Nature* **421**, 611 (Feb. 2003).

[3] Hentschel, M., Kienberger, R., Spielmann, C., Reider, G. A., Milosevic, N., Brabec, T., Corkum, P., Heinzmann, U., Drescher, M., and Krausz, F., "Attosecond metrology," *Nature* **414**, 509 (Nov. 2001).

[4] Christov, I. P., Murnane, M. M., and Kapteyn, H. C., "High-harmonic generation of attosecond pulses in the "single-cycle" regime," *Phys. Rev. Lett.* **78**, 1251 (Feb. 1997).

[5] Goulielmakis, E., Schultze, M., Hofstetter, M., Yakovlev, V. S., Gagnon, J., Uiberacker, M., Aquila, A. L., Gullikson, E. M., Attwood, D. T., Kienberger, R., Krausz, F., and Kleineberg, U., "Single-cycle nonlinear optics," *Science* **320**, 1614 (2008).

[6] Uiberacker, M., Uphues, T., Schultze, M., Verhoef, A. J., Yakovlev, V., Kling, M. F., Rauschenberger, J., Kabachnik, N. M., Schroder, H., Lezius, M., Kompa, K. L., Muller, H.-G., Vrakking, M. J. J., Hendel, S., Kleineberg, U., Heinzmann, U., Drescher, M., and Krausz, F., "Attosecond real-time observation of electron tunnelling in atoms," *Nature* **446**, 627 (Apr. 2007).

[7] Goulielmakis, E., Loh, Z.-H., W., A., Santra, R., Rohringer, N., Yakovlev, V. S., Zherebtsov, S., Pfeifer, T., Azzeer, A. M., Kling, M. F., Leone, S. R., and Krausz, F., "Real-time observation of valence electron motion," *Nature* **466**, 739 (2010).

[8] Schultze, M., Fiess, M., Karpowicz, N., Gagnon, J., Korbman, M., Hofstetter, M., Neppl, S., Cavalieri, A. L., Komninos, Y., Mercouris, T., Nicolaides, C. A., Pazourek, R., Nagele, S., Feist, J., Burgdörfer, J., Azzeer, A. M., Ernstorfer, R., Kienberger, R., Kleineberg, U., Goulielmakis, E., Krausz, F., and Yakovlev, V. S., "Delay in photoemission," *Science* **328**, 1658 (2010).

[9] Föhlisch, A., Feulner, P., Hennies, F., Fink, A., Menzel, D., Sánchez-Portal, D., Echenique, P. M., and Wurth, W., "Direct observation of electron dynamics in the attosecond domain," *Nature* **436**, 373 (July 2005).

[10] Borisov, A., Sánchez-Portal, D., Díez Muiño, R., and Echenique, P. M., "Building up the screening below the femtosecond scale," *Chem. Phys. Lett.* **387**, 95 (Mar. 2004).

[11] Itatani, J., Quéré, F., Yudin, G. L., Ivanov, M. Y., Krausz, F., and Corkum, P. B., "Attosecond streak camera," *Phys. Rev. Lett.* **88**, 173903 (Apr. 2002).

[12] Kienberger, R., Goulielmakis, E., Uiberacker, M., Baltuška, A., Yakovlev, V., Bammer, F., Scrinzi, A., Westerwalbesloh, T., Kleineberg, U., Heinzmann, U., Drescher, M., and Krausz, F., "Atomic transient recorder," *Nature* **427**, 817 (Feb. 2004).

[13] Cavalieri, A. L., Müller, N., Uphues, T., Yakovlev, V. S., Baltuška, A., Horvath, B., Schmidt, B., Blümel, L., Holzwarth, R., Hendel, S., Drescher, M., Kleineberg, U., Echenique, P. M., Kienberger, R., Krausz, F., and Heinzmann, U., "Attosecond spectroscopy in condensed matter," *Nature* **449**, 1029 (Oct. 2007).

[14] Zhang, C.-H. and Thumm, U., "Attosecond photoelectron spectroscopy of metal surfaces," *Phys. Rev. Lett.* **102**, 123601 (Mar. 2009).

[15] Lemell, C., Solleder, B., Tökési, K., and Burgdörfer, J., "Simulation of attosecond streaking of electrons emitted from a tungsten surface," *Phy. Rev. A* **79**, 062901 (2009).

[16] Kazansky, A. K. and Echenique, P. M., "One-electron model for the electronic response of metal surfaces to subfemtosecond photoexcitation," *Phys. Rev. Lett.* **102**, 177401 (May 2009).

[17] Krasovskii, E. E., "Attosecond spectroscopy of solids: Streaking phase shift due to lattice scattering," *Phys. Rev. B* **84**, 195106 (Nov 2011).

[18] Zhang, C.-H. and Thumm, U., "Streaking and wigner time delays in photoemission from atoms and surfaces," *Phys. Rev. A* **84**, 033401 (Sep 2011).

[19] Neppl, S., Ernstorfer, R., Bothschafter, E. M., Cavalieri, A. L., Menzel, D., Barth, J. V., Krausz, F., Kienberger, R., and Feulner, P., "Attosecond time-resolved photoemission from core and valence states of magnesium," *Phys. Rev. Lett.* **109**, 087401 (Aug 2012).

[20] Cavalieri, A. L., Goulielmakis, E., Horvath, B., Helml, W., Schultze, M., Fieß, M., Pervak, V., Veisz, L., Yakovlev, V. S., Uiberacker, M., Apolonski, A., Krausz, F., and Kienberger, R., "Intense 1.5-cycle near infrared laser waveforms and their use for the generation of ultra-broadband soft-x-ray harmonic continua," *New J. Phys.* **9**, 242 (2007).

[21] Magerl, E., Neppl, S., Cavalieri, A. L., Bothschafter, E. M., Stanislawski, M., Uphues, T., Hofstetter, M., Kleineberg, U., Barth, J. V., Menzel, D., Krausz, F., Ernstorfer, R., Kienberger, R., and Feulner, P., "A flexible apparatus for attosecond photoelectron spectroscopy of solids and surfaces," *Rev. Sci. Instr.* **82**, 063104 (2011).

[22] Corkum, P., "Plasma perspective on strong field multiphoton ionization," *Phys. Rev. Lett.* **71**, 1994 (Sept. 1993).

[23] Gagnon, J., Goulielmakis, E., and Yakovlev, V., "The accurate frog characterization of attosecond pulses from streaking measurements," *Appl. Phys. B* **92**, 25 (2008). 10.1007/s00340-008-3063-x.

[24] Zhang, C.-H. and Thumm, U., "Effect of wave-function localization on the time delay in photoemission from surfaces," *Phys. Rev. A* **84**, 065403 (Dec 2011).

[25] Zhang, C.-H. and Thumm, U., "Probing dielectric-response effects with attosecond time-resolved streaked photoelectron spectroscopy of metal surfaces," *Phys. Rev. A* **84**, 063403 (Dec 2011).

[26] Bartynski, R. A., Gaylord, R. H., Gustafsson, T., and Plummer, E. W., "Angle-resolved photoemission study of the surface and bulk electronic structure of mg(0001) and mg(112-bar0)," *Phys. Rev. B* **33**, 3644 (Mar. 1986).

[27] Schiller, F., Heber, M., Servedio, V. D. P., and Laubschat, C., "Electronic structure of mg : From monolayers to bulk," *Phys. Rev. B* **70**, 125106 (Sept. 2004).

[28] Krasovskii, E. E., Silkin, V. M., Nazarov, V. U., Echenique, P. M., and Chulkov, E. V., "Dielectric screening and band-structure effects in low-energy photoemission," *Phys. Rev. B* **82**, 125102 (Sep 2010).

[29] Karlsson, U. O., Hansson, G. V., Persson, P. E. S., and Flodström, S. A., "Surface electronic structure of mg(0001)," *Phys. Rev. B* **26**, 1852 (Aug. 1982).

[30] Penn, D. R., "Role of intrinsic plasmons in conduction-band x-ray photoemission from solids," *Phys. Rev. Lett.* **40**, 568 (Feb. 1978).

[31] Shirley, D., "High-resolution x-ray photoemission spectrum of the valence band of gold," *Phys. Rev.* **5**, 4709 (1972).

[32] Palik, E., [*Handbook of Optical Constants of Solids*], Academic Press Inc (1991).

[33] Tanuma, S., Powell, C. J., and Penn, D. R., "Calculations of electron inelastic mean free paths. ix. data for 41 elemental solids over the 50 ev to 30 kev range," *Surface and Interface Analysis* **43**, 689 (2011).

[34] Germer, L. and May, J., "Diffraction study of oxygen adsorption on a (110) tungsten face," *Surface Science* **4**, 452 (1966).

[35] Ynzunza, R. X., Palomares, F. J., Tober, E. D., Wang, Z., Morais, J., Denecke, R., Daimon, H., Chen, Y., Hussain, Z., Hove, M. A. V., and Fadley, C. S., "Structure determination for saturated (11) oxygen on w(110) from full solid angle photoelectron diffraction with chemical-state resolution," *Surface Science* **442**, 27 (1999).

[36] Daimon, H., Ynzunza, R., Palomares, J., Takabi, H., and Fadley, C. S., "Direct structure analysis of w(110)-(11)-o by full solid-angle x-ray photoelectron diffraction with chemical-state resolution," *Surface Science* **408**, 260 (1998).

[37] Johnson, K. E., Wilson, R. J., and Chiang, S., "Effects of adsorption site and surface stress on ordered structures of oxygen adsorbed on w(110)," *Phys. Rev. Lett.* **71**, 1055 (1993).

[38] Neppl, S., *Attosecond Time-Resolved Photoemission from Surfaces and Interfaces*, phD Thesis, Technische Universität München (2012).